



Ultrashort polarization-tailored bichromatic fields from a CEP-stable white light supercontinuum

STEFANIE KERBSTADT, DANIEL TIMMER, LARS ENGLERT, TIM BAYER, AND MATTHIAS WOLLENHAUPT*

Institute of Physics, Carl von Ossietzky University, Oldenburg, Germany

*matthias.wollenhaupt@uni-oldenburg.de

Abstract: We apply ultrafast polarization shaping to an ultrabroadband carrier envelope phase (CEP) stable white light supercontinuum to generate polarization-tailored bichromatic laser fields of low-order frequency ratio. The generation of orthogonal linearly and counter-rotating circularly polarized bichromatic fields is achieved by introducing a composite polarizer in the Fourier plane of a $4f$ polarization shaper. The resulting Lissajous- and propeller-type polarization profiles are characterized experimentally by cross-correlation trajectories. The scheme provides full control over all bichromatic parameters and allows for individual spectral phase modulation of both colors. Shaper-based CEP control and the generation of tailored bichromatic fields is demonstrated. These bichromatic CEP-stable polarization-shaped ultrashort laser pulses provide a versatile class of waveforms for coherent control experiments.

© 2017 Optical Society of America

OCIS codes: (320.5540) Pulse shaping; (320.6629) Supercontinuum generation; (320.5520) Pulse compression; (320.7100) Ultrafast measurements.

References and links

1. D. B. Milošević and W. Becker, "Attosecond pulse trains with unusual nonlinear polarization," *Phys. Rev. A* **62**, 011403R (2000).
2. O. Kfir, P. Grychtol, E. Turgut, R. Knut, D. Zusin, D. Popmintchev, T. Popmintchev, H. Nembach, J. M. Shaw, A. Fleischer, H. Kapteyn, M. Murnane, and O. Cohen, "Generation of bright phase-matched circularly-polarized extreme ultraviolet high harmonics," *Nature Phot.* **9**, 99–105 (2015).
3. J. M. Ngoko Djiokap, A. V. Meremianin, N. L. Manakov, S. X. Hu, L. B. Madsen, and A. F. Starace, "Multistart spiral electron vortices in ionization by circularly polarized UV pulses," *Physical Review A* **94**, 013408 (2016).
4. E. Hasović, W. Becker, and D. B. Milošević, "Electron rescattering in a bicircular laser field," *Optics Express* **24**, 6413–6424 (2016).
5. S. Eckart, M. Richter, M. Kunitski, A. Hartung, J. Rist, K. Henrichs, N. Schlott, H. Kang, T. Bauer, H. Sann, L. P. H. Schmidt, M. Schöffler, T. Jahnke, and R. Dörner, "Nonsequential double ionization by counterrotating circularly polarized two-color laser fields," *Physical Review Letters* **117**, 133202 (2016).
6. C. A. Mancuso, K. M. Dorney, D. D. Hickstein, J. L. Chaloupka, J. L. Ellis, F. J. Dollar, R. Knut, P. Grychtol, D. Zusin, C. Gentry, M. Gopalakrishnan, H. C. Kapteyn, and M. M. Murnane, "Controlling nonsequential double ionization in two-color circularly polarized femtosecond laser fields," *Physical Review Letters* **117**, 133201 (2016).
7. H. Ohmura, N. Saito, and M. Tachiya, "Selective ionization of oriented nonpolar molecules with asymmetric structure by phase-controlled two-color laser fields," *Phys. Rev. Lett.* **96**, 173001 (2006).
8. D. Ray, F. He, S. De, W. Cao, H. Mashiko, P. Ranitovic, K. P. Singh, I. Znakovskaya, U. Thumm, G. G. Paulus, M. F. Kling, I. V. Litvinyuk, and C. L. Cocke, "Ion-energy dependence of asymmetric dissociation of D_2 by a two-color laser field," *Phys. Rev. Lett.* **103**, 223201 (2009).
9. K.-J. Yuan and A. D. Bandrauk, "Interference asymmetry of molecular frame photoelectron angular distributions in bichromatic uv ionization processes," *Journal of Physics B: Atomic, Molecular and Optical Physics* **49**, 065601 (2016).
10. E. Dupont, P. B. Corkum, H. C. Liu, M. Buchanan, and Z. R. Wasilewski, "Phase-controlled currents in semiconductors," *Phys. Rev. Lett.* **74**, 3596–3599 (1995).
11. L. Costa, M. Betz, M. Spasenović, A. D. Bristow, and H. M. Van Driel, "All-optical injection of ballistic electrical currents in unbiased silicon," *Nature Phys.* **3**, 632–635 (2007).
12. J. Güdde, M. Rohleder, T. Meier, S. W. Koch, and U. Höfer, "Controlled electric currents at a metal surface time-resolved investigation of coherently," *Science* **318**, 1287–1291 (2007).
13. M. Shapiro and P. Brumer, *Quantum Control of Molecular Processes*, 2nd ed. (Wiley, 2012).

14. S. Kerbstadt, L. Englert, T. Bayer, and M. Wollenhaupt, "Ultrashort polarization-tailored bichromatic fields," *J. Mod. Opt.* (published online) (2016), DOI: 10.1080/09500340.2016.1271151.
15. J. Köhler, M. Wollenhaupt, T. Bayer, C. Sarpe, and T. Baumert, "Zeptosecond precision pulse shaping," *Opt. Express* **19**, 11638–11653 (2011).
16. B. Xu, Y. Coello, V. V. Lozovoy, D. A. Harris, and M. Dantus, "Pulse shaping of octave spanning femtosecond laser pulses," *Opt. Express* **14**, 10939–10944 (2006).
17. S. Rausch, T. Binhammer, A. Harth, F. X. Kärtner, and U. Morgner, "Few-cycle femtosecond field synthesizer," *Opt. Express* **16**, 17410–17419 (2008).
18. F. Hagemann, O. Gause, L. Wöste, and T. Siebert, "Supercontinuum pulse shaping in the few-cycle regime," *Opt. Express* **21**, 5536–5549 (2013).
19. H.-S. Chan, Z.-M. Hsieh, W.-H. Liang, A. H. Kung, C.-K. Lee, C.-J. Lai, R.-P. Pan, L.-H. Peng, "Synthesis and Measurement of Ultrafast Waveforms from Five Discrete Optical Harmonics," *Science* **318**, 1287–1291 (2007).
20. C. Manzoni, O. D. Mücke, G. Cirmi, S. Fang, J. Moses, S.-W. Huang, K.-H. Hong, G. Cerullo, and F. X. Kärtner, "Coherent pulse synthesis: towards sub-cycle optical waveforms," *Laser Photonics Rev.* **9**, 129–171 (2015).
21. T. Brixner and G. Gerber, "Femtosecond polarization pulse shaping," *Opt. Lett.* **26**, 557–559 (2001).
22. A. M. Weiner, "Femtosecond pulse shaping using spatial light modulators," *Rev. Sci. Instrum.* **71**, 1929–1960 (2000).
23. D. Pengel, S. Kerbstadt, D. Johannmeyer, L. Englert, T. Bayer, and M. Wollenhaupt, "Electron vortices in femtosecond multiphoton ionization," *Phys. Rev. Lett.* **118**, 053003 (2017).
24. A. Präkelt, M. Wollenhaupt, A. Assion, C. Horn, C. Sarpe-Tudoran, M. Winter, and T. Baumert, "Compact, robust and flexible setup for femtosecond pulse shaping," *Rev. Sci. Instrum.* **74**, 4950–4953 (2003).
25. V. V. Lozovoy, I. Pastirk, and M. Dantus, "Multiphoton intrapulse interference. iv. ultrashort laser pulse spectral phase characterization and compensation," *Opt. Lett.* **29**, 1–3 (2004).
26. B. von Vacano, T. Backup, and M. Motzkus, "In situ broadband pulse compression for multiphoton microscopy using a shaper-assisted collinear spider," *Opt. Lett.* **31**, 1154–1156 (2006).
27. A. Galler and T. Feuer, "Pulse shaper assisted short laser pulse characterization," *Appl. Phys. B* **90**, 427–430 (2008).
28. M. Wollenhaupt, M. Krug, J. Köhler, T. Bayer, C. Sarpe-Tudoran, and T. Baumert, "Photoelectron angular distributions from strong-field coherent electronic excitation," *Appl. Phys. B* **95**, 245–259 (2009).
29. L. Polachek, D. Oron, and Y. Silberberg, "Full control of the spectral polarization of ultrashort pulses," *Opt. Lett.* **31**, 631–633 (2006).
30. M. Ninck, A. Galler, T. Feuer, and T. Brixner, "Programmable common-path vector field synthesizer for femtosecond pulses," *Opt. Lett.* **32**, 3379–3381 (2007).
31. F. Weise and A. Lindinger, "Full control over the electric field using four liquid crystal arrays," *Opt. Lett.* **34**, 1258–1256 (2009).
32. D. Kupka, P. Schlup, and R. A. Bartels, "Simplified ultrafast pulse shaper for tailored polarization states using a birefringent prism," *Rev. Sci. Instrum.* **80**, 053110 (2009).
33. C.-C. Chen, I.-C. Hsieh, S.-D. Yang, and C.-B. Huang, "Polarization line-by-line pulse shaping for the implementation of vectorial temporal Talbot effect," *Opt. Express* **20**, 27062–27070 (2012).
34. C. Schwarz, O. Hüter, and T. Brixner, "Full vector-field control of ultrashort laser pulses utilizing a single dual-layer spatial light modulator in a common-path setup," *JOSA B* **32**, 933–945 (2015).
35. A. Monmayrant, S. Weber, and B. Chatel, "A newcomer's guide to ultrashort pulse shaping and characterization," *J. Phys. B* **43**, 103001 (2010).
36. T. Baumert, T. Brixner, V. Seyfried, M. Strehle, and G. Gerber, "Femtosecond pulse shaping by an evolutionary algorithm with feedback," *Appl. Phys. B* **65**, 779–782 (1997).
37. D. Yelin, D. Meshulach, and Y. Silberberg, "Adaptive femtosecond pulse compression," *Opt. Lett.* **22**, 1793–1795 (1997).
38. A. Monmayrant, B. Chatel, and B. Girard, "Femtosecond spectral electric field reconstruction using coherent transients," *Optics Letters* **31**, 410–412 (2006).
39. A. M. Weiner, D. E. Leaird, G. P. Wiederrecht, and K. A. Nelson, "Femtosecond pulse sequences used for optical manipulation of molecular motion," *Science* **247**, 1317–1319 (1990).
40. A. Bartelt, A. Lindinger, C. Lupulescu, S. Vajda, and L. Wöste, "One parameter fs-pulse form control on NaK and Na₂K," *Phys. Chem. Chem. Phys.* **5**, 3610–3615 (2003).
41. N. Dudovich, D. Oron, and Y. Silberberg, "Single-pulse coherent anti-stokes raman spectroscopy in the fingerprint spectral region," *J. Chem. Phys.* **118**, 9208–9215 (2003).
42. W. Wohlleben, T. Backup, J. L. Herek, and M. Motzkus, "Coherent control for spectroscopy and manipulation of biological dynamics," *Chem. Phys. Chem.* **6**, 850–857 (2005).
43. M. Wollenhaupt, A. Präkelt, C. Sarpe-Tudoran, D. Liese, T. Bayer, and T. Baumert, "Femtosecond strong-field quantum control with sinusoidally phase-modulated pulses," *Phys. Rev. A* **73**, 063409 (2006).
44. P. B. Corkum and F. Krausz, "Attosecond science," *Nature Phys.* **3**, 381–387 (2007).
45. M. F. Kling and M. J. J. Vrakking, "Attosecond electron dynamics," *Ann. Rev. Phys. Chem.* **59**, 463–499 (2008).
46. F. Krausz and M. Ivanov, "Attosecond physics," *Rev. Mod. Phys.* **81**, 163–234 (2009).
47. M. Abel, D. M. Neumark, S. R. Leone, and T. Pfeifer, "Classical and quantum control of electrons using the carrier-envelope phase of strong laser fields," *Laser Photonics Rev.* **5**, 352–367 (2011).
48. R. Kienberger, E. Goulielmakis, M. Uiberacker, A. Baltuska, V. Yakolev, F. Bammer, A. Scrinzi, T. Westerwalbesloh,

- U. Kleineberg, U. Heinzmann, M. Drescher, and F. Krausz, "Atomic transient recorder," *Nature* **427**, 817–821 (2004).
49. I. J. Sola, E. Mével, L. Elouga, E. Constant, V. Strelkov, L. Poletto, P. Villoresi, E. Benedetti, J. P. Caumes, S. Stagira, C. Vozzi, G. Sansone, and M. Nisoli, "Controlling attosecond electron dynamics by phase-stabilized polarization gating," *Nature Phys.* **2**, 319–322 (2006).
50. C. A. Haworth, L. E. Chipperfield, J. S. Robinson, P. L. Knight, J. P. Marangos, and J. W. G. Tisch, "Half-cycle cutoffs in harmonic spectra and robust carrier-envelope phase retrieval," *Nat Phys* **3**, 52–57 (2007).
51. T. Pfeifer, M. J. Abel, P. M. Nagel, W. Boutu, M. J. Bell, Y. Liu, D. M. Neumark, and S. R. Leone, "Measurement and optimization of isolated attosecond pulse contrast," *Optics Letters* **34**, 1819–1821 (2009).
52. M. F. Kling, J. Rauschenberger, A. J. Verhoef, E. Hasović, T. Uphues, D. B. Milošević, H. G. Muller, and M. J. J. Vrakking, "Imaging of carrier-envelope phase effects in above-threshold ionization with intense few-cycle laser fields," *New J. Phys.* **10**, 025024 (2008).
53. M. F. Kling, C. Siedschlag, A. J. Verhoef, J. I. Khan, M. Schultze, T. Uphues, Y. Ni, M. Uiberacker, M. Drescher, F. Krausz, and M. J. J. Vrakking, "Control of electron localization in molecular dissociation," *Science* **312**, 246–248 (2006).
54. M. Vrakking, "Chemical physics electronic movies," *Nature* **460**, 960–961 (2009).
55. A. M. Weiner, "Ultrafast optical pulse shaping: A tutorial review," *Opt. Comm.* **284**, 3669–3692 (2011).
56. M. Wollenhaupt, T. Bayer, and T. Baumert, *Control of Ultrafast Electron Dynamics with Shaped Femtosecond Laser Pulses: From Atoms to Solids* (Springer, 2015), book section 4, pp. 63–122.
57. C. Lux, M. Wollenhaupt, T. Bolze, Q. Liang, J. Köhler, C. Sarpe, and T. Baumert, "Circular dichroism in the photoelectron angular distributions of camphor and fenchone from multiphoton ionization with femtosecond laser pulses," *Angew. Chem. Int. Ed.* **51**, 5001–5005 (2012).

1. Introduction

Ultrashort bichromatic laser fields have emerged as a new twist to coherently control ultrafast electron dynamics in atoms [1–6], molecules [7–9] and solids [10–12]. In recent years, $(\omega : 2\omega)$ -fields have been employed in numerous applications to observe and manipulate the motion of electron wave packets on their intrinsic timescales. The physical mechanism behind bichromatic control is based on the interference between M -photon and N -photon excitation pathways, where M and N are (small) integer numbers [13]. In order to exploit the full potential of bichromatic control, the availability of bichromatic fields with low-order commensurable frequencies of adjustable ratio is therefore highly desirable. Typically, $(\omega : 2\omega)$ -fields are generated by superimposing a fundamental laser beam with its second harmonic. Recently, we demonstrated an alternative route to the generation of polarization-tailored bichromatic fields based on ultrafast polarization pulse shaping techniques [14]. The scheme allows to tune all bichromatic parameters, such as the frequency ratio, amplitude ratio, bandwidth and helicity of the two colors. In addition, the phase of both spectral bands can independently be modulated which allows to adjust the relative phase and time delay of the two colors with zeptosecond precision [15] or, in general, to generate tailor-made bichromatic fields. Due to the limited bandwidth of the pulses used in [14], however, the generation of low-order commensurable bichromatic fields has not been shown so far. In this contribution, we apply the scheme to an octave-spanning white light supercontinuum (WLS) from a carrier envelope phase (CEP) stabilized WL source and demonstrate the generation of ultrashort polarization-tailored bichromatic fields with variable frequency ratios $(M\omega : N\omega)$, for small integer numbers M and N . Demonstrations of WL pulse shaping have been reported in [16–18], including the synthesis of few-cycle waveforms from discrete optical harmonics [19]. The latter has recently been reviewed in [20]. Shaper-based control of the CEP was demonstrated in [17]. So far, however, the CEP stability of the shaped output pulses was not investigated. Here we show, that our setup maintains the CEP stability making the approach especially attractive for few-cycle coherent control applications.

Our approach utilizes a $4f$ polarization pulse shaper [21] based on the classic design by A. Weiner [22] equipped with a dual-layer liquid crystal spatial light modulator (LC-SLM). In amplitude and phase modulation mode, the shaper allows us to sculpture the bichromatic amplitude profile directly from the given input spectrum. Employing a linear polarizer in the Fourier plane of the $4f$ setup, the scheme yields parallel linearly polarized (P-LP) bichromatic output fields which, by additional insertion of a $\lambda/4$ wave plate (QWP), are converted into

co-rotating circularly polarized (COR-CP) bichromatic fields. For the generation of orthogonal linearly polarized (O-LP) and counter-rotating circularly polarized (CNR-CP) bichromatic fields, we modified the shaper layout by introducing a composite polarizer in the Fourier plane. The composite polarizer consists of two adjacent areas with orthogonal transmission directions, horizontally aligned such that the low frequency part of the spectrum is *s*-polarized while the high frequency part is *p*-polarized. By this means, two orthogonally polarized spectral bands are independently phase- and amplitude-modulated yields polarization-shaped O-LP fields at the shaper output. The O-LP output fields can be converted to CNR-CP fields using a QWP, as illustrated in Fig. 1. So far, single-color CNR-CP pulses have been employed to demonstrate free electron vortices in the multi-photon ionization of potassium atoms [23].

Being based on a common-path setup [24–28], our scheme provides inherent phase stability of the two colors. In addition, the scheme features built-in dispersion management and allows for shaper-based pulse characterization by spectral phase and amplitude modulation [14, 25, 27]. Recently, various common-path setups have been proposed for full vector control over the electric field of ultrashort laser pulses [29–34]. The approach presented here is specifically tailored to the generation of polarization-shaped bichromatic fields. It is comparably cost-efficient as it relies on only two LC-layers. Furthermore, the scheme makes use of the full spatial range of the SLM (640 pixels) to cover the laser spectrum, providing maximum spectral resolution particularly important for ultrabroadband applications.

The paper is organized as follows. We start by describing the experimental scheme for shaper-based generation and characterization of polarization-tailored bichromatic fields sculptured from an octave-spanning input WLS. In the experiments, we focus on O-LP and CNR-CP fields to highlight the new concept based on a composite polarizer. First, we demonstrate the generation of bandwidth-limited CNR-CP fields with low-order commensurable frequencies supported by the bandwidth of the WLS. Next, individual spectral phase modulation is applied to both colors and the generation of high-fidelity bichromatic fields with tailored amplitude, phase and polarization profiles is demonstrated. Finally, the CEP stability of the generated fields is investigated and shaper-based control of the CEP is demonstrated.

2. Experimental

2.1. Setup

The experimental setup is sketched in Fig. 1. We use a home-built grating-based polarization pulse shaper in $4f$ geometry with dual-layer LC-SLM (*Jenoptik*, SLM-S640d), consisting of two LC displays referred to as LCD A and LCD B, for independent spectral amplitude and phase modulation of an octave-spanning WLS generated in an Argon-filled hollow-core fiber (HF) (*Femtolasers* Kaleidoscope). In order to adapt the shaper setup to the ultrabroadband WLS, we first performed a phase calibration of the LC-SLM [22] using a narrowband laser diode at a wavelength of about 800 nm. The calibration is converted to the full spectral range (430–1100 nm) using the wavelength-dependent optical anisotropy of the LCs, as provided by the manufacturer and described in [35]. With the phase calibration available, the non-linear wavelength-to-pixel relation is determined *in situ* by amplitude modulation of the WLS. To this end, we initially use the analytic expression for the spatial dispersion of the gratings to set all but one pixel dark. By scanning the bright pixel across the LC-SLM and measuring the output with a spectrometer (*Avantes* AVASPEC-ULS3648-RS-USB2), a refined relation is obtained which is finally used in the experiments. To eliminate higher diffraction orders in the Fourier plane, an order sorting filter is mounted in front of the LC-SLM. The HF is seeded by 790 nm, 20-fs pulses from an actively CEP-stabilized laser system (*Femtolasers* Femtopower HR 3 kHz CEP with Rainbow 500 oscillator and CEP4 module). The seed pulse energy was set to 500 μ J and the Ar gas pressure was adjusted to 0.5 bar. No additional chirped mirrors are used to compress the output of the HF. Pulse compression is performed by employing the shaper to adaptively optimize the

second harmonic generation (SHG) in a β -barium borate (BBO) crystal (*EKSMA*, $\theta = 29.2^\circ$, $5 \mu\text{m}$ thickness) behind the setup [see Fig. 1] using an evolutionary algorithm [14, 36, 37]. By this means, the entire dispersion introduced in the beamline between laser system and experiment is compensated. The long-term CEP stability of the WLS was measured using a home-built f - $2f$ -interferometer yielding CEP fluctuations of about 270 mrad root mean square (RMS) over a period of 1 h. At the shaper output, we obtain CEP-stable few-cycle pulses with a duration of about $\Delta t = 5.3$ fs.

For the generation of polarization-shaped bichromatic fields, a composite polarizer (*Codixx*, ColorPol[®]) is mounted behind the LC-SLM close to the Fourier plane [see Fig. 1]. By this means, the spectrum is split into two orthogonally polarized bands at a splitting frequency denoted by ω_0 . Then combined amplitude and phase modulation of the two bands is implemented by the phase modulation functions

$$\varphi_A(\omega) = \begin{cases} \varphi_1(\omega) - \arccos\left(\frac{A_1(\omega)}{\tilde{E}_{in}(\omega)}\right), & \omega < \omega_0 \\ \varphi_2(\omega) + \arccos\left(\frac{A_2(\omega)}{\tilde{E}_{in}(\omega)}\right), & \omega \geq \omega_0 \end{cases} \quad (1)$$

and

$$\varphi_B(\omega) = \begin{cases} \varphi_1(\omega) - \arccos\left(-\frac{A_1(\omega)}{\tilde{E}_{in}(\omega)}\right), & \omega < \omega_0 \\ \varphi_2(\omega) - \arccos\left(\frac{A_2(\omega)}{\tilde{E}_{in}(\omega)}\right), & \omega \geq \omega_0 \end{cases} \quad (2)$$

applied to LCDs A and B, respectively [14]. Here, $\tilde{E}_{in}(\omega)$ is the spectral amplitude of the WL input pulse, assumed to be real-valued, $A_{1/2}(\omega)$ are the amplitude modulation profiles of the bichromatic target spectrum centered at $\omega_1 < \omega_0$ and $\omega_2 > \omega_0$, respectively, and $\varphi_{1/2}(\omega)$ are the phase modulation functions for each spectral band. In this configuration, the setup delivers O-LP bichromatic fields at the shaper output. If required, the O-LP fields are converted into CNR-CP bichromatic fields by additional use of a super-achromatic QWP (*B. Halle Nachfl.*, 300-1100 nm) behind the setup.

2.2. Characterization

For the temporal characterization of the generated bichromatic fields, we employ a shaper-based cross-correlation (CC) technique [14, 15, 27, 38]. A bandwidth-limited reference pulse is split off the input pulse by additional spectral phase and amplitude modulation using the phase modulation functions

$$\varphi_A(\omega) = \begin{cases} \varphi'_1(\omega) - \arccos\left[\frac{A_1(\omega)}{\tilde{E}_{in}(\omega)} \cos(\varphi''_1(\omega))\right], & \omega < \omega_0 \\ \varphi'_2(\omega) + \arccos\left[\frac{A_2(\omega)}{\tilde{E}_{in}(\omega)} \cos(\varphi''_2(\omega))\right], & \omega \geq \omega_0 \end{cases} \quad (3)$$

and

$$\varphi_B(\omega) = \begin{cases} \varphi'_1(\omega) - \arccos\left[-\frac{A_1(\omega)}{\tilde{E}_{in}(\omega)} \cos(\varphi''_1(\omega))\right], & \omega < \omega_0 \\ \varphi'_2(\omega) - \arccos\left[\frac{A_2(\omega)}{\tilde{E}_{in}(\omega)} \cos(\varphi''_2(\omega))\right], & \omega \geq \omega_0 \end{cases}, \quad (4)$$

with

$$\varphi'_n(\omega) = \frac{\varphi_n(\omega) + \varphi_{ref,n}(\omega)}{2} \quad \text{and} \quad \varphi''_n(\omega) = \frac{\varphi_n(\omega) - \varphi_{ref,n}(\omega)}{2}, \quad n = 1, 2. \quad (5)$$

Application of the phase functions in Eqs. (3) and (4) yields the modulated output field

$$\tilde{\mathbf{E}}_{mod}^+(\omega) = \frac{1}{2} \begin{pmatrix} A_1(\omega) \left[e^{-i\varphi_1(\omega)} + e^{-i\varphi_{ref,1}(\omega)} \right] \\ A_2(\omega) \left[e^{-i\varphi_2(\omega)} + e^{-i\varphi_{ref,2}(\omega)} \right] \end{pmatrix}, \quad (6)$$

consisting of the phase-modulated O-LP sample pulse and an O-LP reference pulse modulated by the linear phase

$$\varphi_{ref,n}(\omega) = \varphi_{0,n} + \tau \cdot (\omega - \omega_{ref,n}). \quad (7)$$

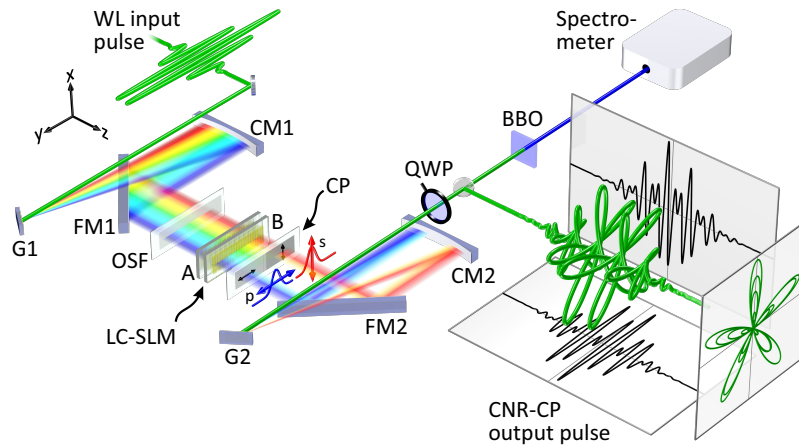


Fig. 1. Optical scheme for the generation of polarization-tailored bichromatic fields. The setup is based on a $4f$ polarization pulse shaper equipped with dual-layer LC-SLM (LCDs A and B). An order sorting filter (OSF) is mounted in front of LCD A to avoid interference with higher diffraction orders from grating G1. The composite polarizer (CP) mounted behind LCD B enables independent amplitude and phase modulation of two orthogonally polarized bands from the octave-spanning input WLS. The superachromatic QWP at the shaper output (optionally) converts the O-LP output field into a CNR-CP bichromatic field. As exemplified on a $(2\omega : 3\omega)$ -field, commensurable center frequencies result in propeller-type pulses. The SHG signal of the output pulses from a BBO crystal is detected both for adaptive pulse compression and pulse characterization. For simplicity, an already compressed WL pulse is depicted at the shaper input. Optical components: G: Grating, CM: Cylindrical mirror, FM: Folding mirror.

The linear term shifts the reference pulse in time by a variable time delay τ . By choice of the reference frequencies $\omega_{ref,n}$ different CC modes are addressed [14, 27]. In the bichromatic case, three distinct modes are (i) $\omega_{ref,n} = 0$, which yields the interferometric CC, (ii) $\omega_{ref,n} = \omega_n$, resulting in the total envelope of the interferometric CC, and (iii) $\omega_{ref,n} = (\omega_2 + \omega_1)/2$, in which case the CC trace follows the beating of the two colors [see e.g. Fig. 2(e)]. The offset phases $\varphi_{0,n}$ in Eq. (7) determine whether the field's in-phase ($\varphi_{0,n} = 0, \pi$) or quadrature components ($\varphi_{0,n} = \pi/2, 3\pi/2$) are measured.

In order to characterize the polarization-shaped output fields temporally, we measure second order CCs of two orthogonal field components (s and p). To this end, we send the pulses into the BBO crystal, aligned either for efficient s - or p -conversion, and detect the SHG signal as a function of τ using the spectrometer, as depicted in Fig. 1. For the characterization of the instantaneous polarization state, we introduce the concept of parametric first order CC trajectories (CCTs). The CCTs reflect the forward projection of the pulse [see e.g. Fig. 2]. The concept is especially useful in the case of commensurable bichromatic fields, where the forward projection reveals the symmetry of the field. To see this, we consider a bandwidth-limited CNR-CP field. For simplicity the two colors are assumed to have the same spectral amplitude profile described by a shape function $\tilde{\mathcal{E}}(\omega)$ centered around $\omega = 0$ and shifted to the respective center frequencies, i.e. $A_n(\omega) = \tilde{\mathcal{E}}(\omega - \omega_n)$. Furthermore, we assume spectral separation of the two colors, i.e. that the center frequency difference $\omega_2 - \omega_1$ is larger than the spectral width $\Delta\omega$ of $\tilde{\mathcal{E}}(\omega)$. The CNR-CP field in frequency domain then reads

$$\tilde{\mathbf{E}}^+(\omega) = \begin{pmatrix} \tilde{E}_x^+(\omega) \\ \tilde{E}_y^+(\omega) \end{pmatrix} = \frac{1}{\sqrt{2}} \begin{pmatrix} 1 & i \\ i & 1 \end{pmatrix} \begin{pmatrix} \tilde{\mathcal{E}}(\omega - \omega_1) \\ \tilde{\mathcal{E}}(\omega - \omega_2) \end{pmatrix} = \frac{1}{\sqrt{2}} \begin{pmatrix} \tilde{\mathcal{E}}(\omega - \omega_1) + i\tilde{\mathcal{E}}(\omega - \omega_2) \\ i\tilde{\mathcal{E}}(\omega - \omega_1) + \tilde{\mathcal{E}}(\omega - \omega_2) \end{pmatrix}. \quad (8)$$

Here the matrix describes the QWP with optical axis aligned at 45° relative to both O-LP components. The corresponding (real-valued) field in time domain is obtained by application of the Fourier shift theorem as

$$\mathbf{E}(t) = \begin{pmatrix} E_x(t) \\ E_y(t) \end{pmatrix} = \mathcal{E}(t) \begin{pmatrix} \cos(\omega_1 t) - \sin(\omega_2 t) \\ -\sin(\omega_1 t) + \cos(\omega_2 t) \end{pmatrix}, \quad (9)$$

with the temporal envelope $\mathcal{E}(t) = \mathcal{F}^{-1}[\tilde{\mathcal{E}}(\omega)](t)$. For commensurable frequencies $\omega_1 = M \delta\omega$ and $\omega_2 = N \delta\omega$, where $\delta\omega$ is some real-valued frequency unit and $M < N$, the field vector describes propeller-type trajectories in the plane. The propeller exhibits c_s symmetry, with $s = (M + N) / \text{gcd}(M, N)$ and $\text{gcd}(M, N)$ being the greatest common divisor of M and N [see Fig. 2].

Next, we show that first order CCs based on Eqs. (3) and (4) reveal the temporal polarization profile. In our experiments, first order CCs are recorded by measuring the power spectral density (PSD) of the bichromatic output field as a function of τ using a polarizer and the spectrometer. In case of an unmodulated CNR-CP sample pulse, obtained by setting $\varphi_n(\omega) \equiv 0$ in Eq. (6), the output field behind the QWP is given by [14]

$$\tilde{\mathbf{E}}_{mod}^+(\omega; \tau) = \frac{1}{\sqrt{2}} \begin{pmatrix} 1 & i \\ i & 1 \end{pmatrix} \begin{pmatrix} \tilde{\mathcal{E}}(\omega - \omega_1)[1 + e^{-i(\varphi_{0,1} + \omega\tau)}] \\ \tilde{\mathcal{E}}(\omega - \omega_2)[1 + e^{-i(\varphi_{0,2} + \omega\tau)}] \end{pmatrix}. \quad (10)$$

Integrating the τ -dependent spectrometer signal measured in x -direction $|\tilde{\mathbf{E}}_{mod,x}^+(\omega, \tau)|^2$ over all ω , we obtain the CC trace

$$\begin{aligned} C_x(\tau; \varphi_{0,1}, \varphi_{0,2}) &= \int_{-\infty}^{\infty} |\tilde{\mathbf{E}}_{mod,x}^+(\omega, \tau)|^2 d\omega \\ &= \mathcal{A}_0 + \mathcal{A}(\tau) [\cos(\varphi_{0,1} + \omega_1\tau) + \cos(\varphi_{0,2} + \omega_2\tau)], \end{aligned} \quad (11)$$

with $\mathcal{A}(\tau) = \mathcal{F}^{-1}[\tilde{\mathcal{E}}^2(\omega)](\tau)$ being the autocorrelation function of the envelope $\mathcal{E}(t)$ and $\mathcal{A}_0 = \mathcal{A}(0)$. Comparing Eqs. (11) and (9), we see that by appropriate choice of the offset phases $\varphi_{0,n}$, $C_x(\tau; \varphi_{0,1}, \varphi_{0,2})$ reveals both components of the field $\mathbf{E}(t)$. Field and CC differ only in their envelopes $\mathcal{E}(t)$ and $\mathcal{A}(\tau)$. The former, being related to the spectrum $\tilde{\mathcal{E}}(\omega)$, is shorter than the latter associated with the squared spectrum $\tilde{\mathcal{E}}^2(\omega)$. However, there is no significant difference when plotting the CCTs for one beating period. For example, the CC trace obtained by aligning the polarizer in s -direction and measuring $C_x(\tau; \varphi_{0,1}, \varphi_{0,2})$ for $\varphi_{0,1} = 0$ and $\varphi_{0,2} = \pi/2$ essentially yields the s -component $E_x(t)$ of the field. Repeating the measurement for $\varphi_{0,1} = \pi/2$ and $\varphi_{0,2} = 0$ yields the p -component $E_y(t)$ of the field. We note that the procedure discussed here for an unmodulated CNR-CP field is applicable to phase-modulated CNR-CP fields as well. For O-LP fields [cf. Fig. 3] the offset phases are $\varphi_{0,1} = \varphi_{0,2} = 0$ and measurements of both $C_x(\tau; 0, 0)$ and $C_y(\tau; 0, 0)$ are necessary.

2.3. Results

We focus on the generation of O-LP and CNR-CP bichromatic fields with low-order commensurable center frequencies, extracted from an ultrabroadband WLS by phase and amplitude modulation. We start in Sec. 2.3.1 with the generation of bandwidth-limited CNR-CP fields. In Sec. 2.3.2, we present shaped bichromatic fields from individual phase modulation of both spectral bands and demonstrate the fidelity of the setup in generating tailored bichromatic fields. Finally, in Sec. 2.3.3, the CEP stability of the generated fields is investigated and the capability for accurate shaper-based CEP control is demonstrated.

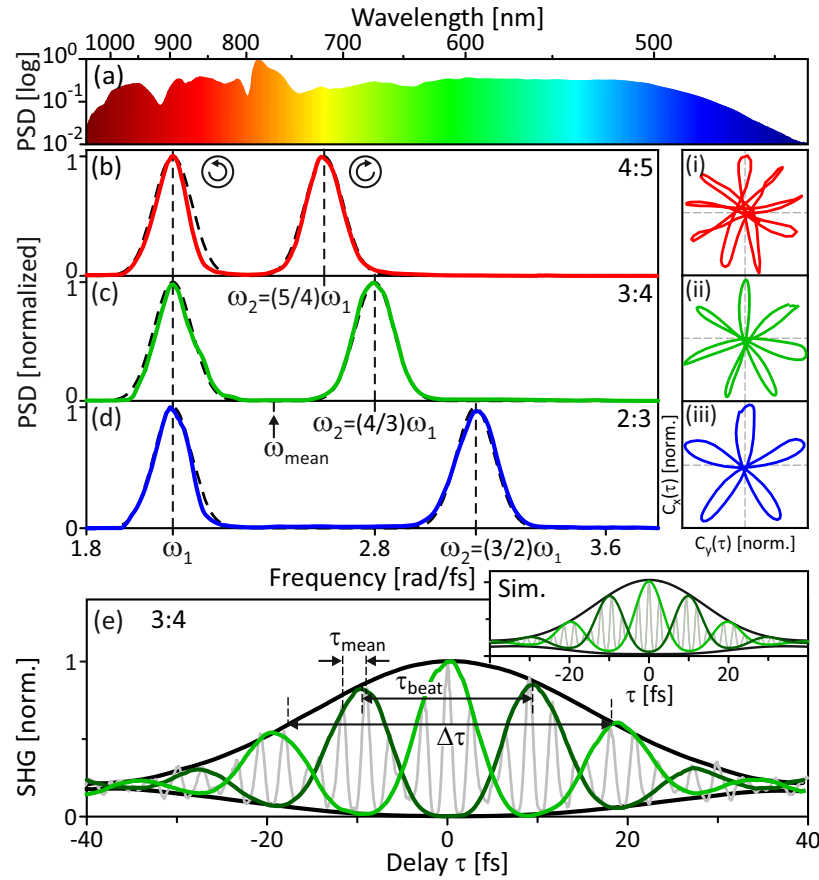


Fig. 2. Gaussian-shaped CNR-CP bichromatic fields with commensurable center frequencies generated by amplitude modulation of the ultrabroadband WLS depicted in (a). Different amplitude profiles with frequency ratios of (b) ($4\omega : 5\omega$), (c) ($3\omega : 4\omega$) and (d) ($2\omega : 3\omega$) are shown. Frames (i)-(iii) display the corresponding temporal polarization profiles in terms of measured CCTs. The CCTs describe propeller-type trajectories with characteristic c_9 , c_7 and c_5 symmetry, respectively. (e) Temporal characterization of the ($3\omega : 4\omega$) field from (c) via shaper-based second order CCs measured in different modes.

2.3.1. Bandwidth-limited CNR-CP bichromatic fields

For the generation of bandwidth-limited bichromatic fields, we set $\varphi_n(\omega) \equiv 0$ in Eqs. (1) and (2). The shaper is used for amplitude modulation and residual phase compensation. Figure 2(a) shows the input WLS. Different Gaussian-shaped bichromatic fields extracted from the WLS with spectral bandwidths of $\Delta\omega_1 = \Delta\omega_2 = \Delta\omega = 0.11$ rad/fs, unity amplitude ratio $A_1/A_2 = 1$ and various combinations of commensurable center frequencies $\omega_1/\omega_2 = M/N$ are depicted in Figs. 2(b)-(d). The center frequency of the low frequency Gaussian was kept fixed at $\omega_1 = 2.10$ rad/fs. The predefined target spectra $A_{1/2}^2(\omega)$ are plotted as black dashed lines to verify the fidelity of the generated amplitude profiles. Using the QWP behind the shaper setup, the O-LP output fields were converted into CNR-CP fields. On the right-hand side of Fig. 2, the temporal polarization profile of the generated fields is illustrated by means of measured CCTs, as shown

in frames (i)-(iii). For clarity, only one beating period of the measured CC traces

$$\mathbf{C}(\tau) = \begin{pmatrix} C_x(\tau) \\ C_y(\tau) \end{pmatrix} = \begin{pmatrix} C_x(\tau; 0, \frac{\pi}{2}) \\ C_x(\tau; \frac{\pi}{2}, 0) \end{pmatrix} \quad (12)$$

is plotted. The measured CCTs reveal propeller-type polarization profiles characteristic for commensurable center frequencies [cf. Eq. (9)]. The frequency ratios of $(4\omega : 5\omega)$, $(3\omega : 4\omega)$ and $(2\omega : 3\omega)$ result in propellers with c_9 [frame (i)], c_7 [frame (ii)] and c_5 symmetry [frame (iii)], respectively.

Figure 2(e) shows the temporal characterization of the $(3\omega : 4\omega)$ -field from Fig. 2(c) by second order CC. The interferometric CC (gray line), measured by setting $\omega_{ref,n} = 0$ and $\varphi_{0,n} = 0$ (for $n = 1, 2$) in Eq. (7), displays the beating of the two colors. The trace oscillates rapidly at the mean frequency $\omega_{mean} = (\omega_1 + \omega_2)/2 = 2.45$ rad/fs, corresponding to a time constant of $\tau_{mean} = 2\pi/\omega_{mean} = 2.6$ fs. The upper and lower envelopes of the beating (green and darkgreen line) were obtained by setting $\omega_{ref,n} = \omega_{mean}$ and $\varphi_{0,n} = 0$ for the upper and $\varphi_{0,n} = \pi$ for the lower envelope. Both traces oscillate slowly at the frequency 0.34 rad/fs corresponding to a period of 18.5 fs. This is in accordance with the expected beating frequency $\omega_{beat} = (\omega_2 - \omega_1)/2 = 0.35$ rad/fs and period $\tau_{beat} = 2\pi/\omega_{beat} = 18.0$ fs. The total envelopes of the pulse (black lines) were measured by setting $\omega_{ref,n} = \omega_n$ and $\varphi_{0,n} = 0$ for the upper and $\varphi_{0,n} = \pi$ for the lower envelope. The full width at half maximum (FWHM) is $\Delta\tau = 35.8$ fs, from which we infer a pulse duration of $\Delta t = \Delta\tau/\sqrt{2} = 25.3$ fs. This value is in excellent agreement with the bandwidth-limit $4 \ln(2)/\Delta\omega = 25.2$ fs of Gaussian-shaped pulses, indicating effective shaper-based pulse compression. For comparison, the inset to Fig. 2(e) shows simulated CC traces calculated on the basis of the experimental pulse parameters.

2.3.2. Tailored O-LP and CNR-CP bichromatic fields

Next we investigate the generation of shaped bichromatic fields. For this purpose, we make use of the phase functions $\varphi_n(\omega)$ (with $n = 1, 2$) in Eqs. (1) and (2) to implement individual spectral phase modulation of both colors. The spectral phase modulation is demonstrated again on the example of a $(3\omega : 4\omega)$ -field as depicted in Fig. 2(c). Figure 3(a) shows the phase-modulated $(3\omega : 4\omega)$ -field in frequency domain. Both colors are modulated by periodic spectral phase functions of the form $\varphi_n(\omega) = a \sin[T_n(\omega - \omega_n)]$. In general, sinusoidal spectral phase modulation results in a temporal sequence of scaled input pulse replica [39–43], with the amplitude of the ν -th sub-pulse determined by the Bessel function $J_\nu(a)$ and the sub-pulse separation given by the sine frequency T_n . For the amplitude of both sine functions, we chose a value of $a = 1.43$ rad for which $J_0(a) = J_1(a)$. Therefore, and taking into account the symmetry relation $J_{-\nu}(a) = (-1)^\nu J_\nu(a)$ of the Bessel function, the resulting pulse sequence in time domain exhibits three central sub-pulses ($\nu = -1, 0, 1$) of equal amplitude, the first pre-pulse ($\nu = -1$) being phase-shifted by π . The time constants of the two sine functions were set to $T_1 = 90$ fs, to ensure non-overlapping sub-pulses, and $T_2 = 2T_1 = 180$ fs.

We start by discussing the modulated O-LP field at the shaper output. In the O-LP case, both colors are disentangled by their polarization directions. Hence, results of a temporal characterization of the s - and p -component via second order CC, shown in Figs. 3(b) and (c), directly reflect the temporal structure of each color. Both measurements display multi-pulse sequences with three central sub-pulses of equal amplitude. The π -phase shift of the respective first pre-pulse is indicated by the upper and lower CC envelopes exchanging their roles. Due to the choice of T_1 and T_2 , the sub-pulse separation of the p -polarized pulse sequence (blue component, ω_2) is twice the separation of the s -polarized sequence (red component, ω_1). This leads to an alternating series of O-LP bichromatic and s -polarized single-color pulses.

The polarization profiles of the individual sub-pulses are illustrated in frames (i)-(v) of Fig. 3 by measured CCTs. For the central main pulse [frame (iii)], where both colors contribute with

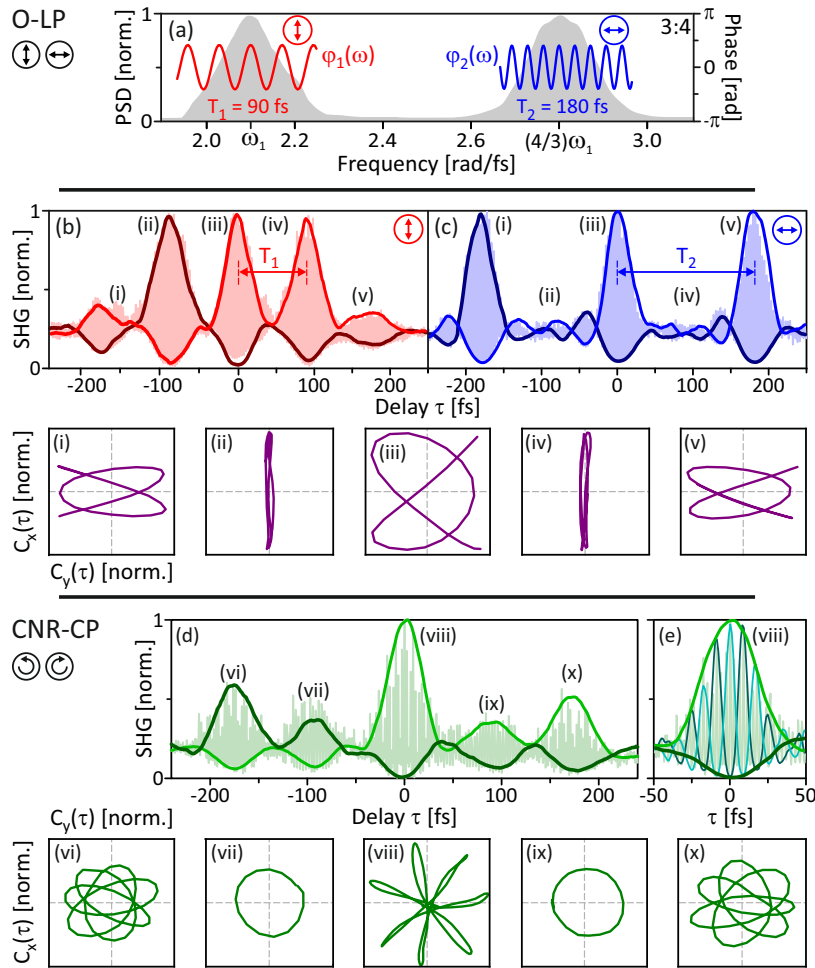


Fig. 3. Bichromatic fields from individual phase modulation of the two orthogonally polarized spectral bands. (a) Bichromatic amplitude profile of a ($3\omega : 4\omega$) O-LP field (gray background) with sinusoidal phase modulation functions $\varphi_1(\omega)$ (red line) and $\varphi_2(\omega)$ (blue lines). (b) and (c) Temporal characterization of the *s*- and *p*-component of the modulated field by second order CC. Measured CCTs of the individual sub-pulses reveal Lissajous-type polarization profiles for the bichromatic sub-pulses shown in frames (i)-(v). (d) In the CNR-CP case, the bichromatic sub-pulses exhibit a beating pattern. The beating is fully modulated in the central sub-pulse shown in (e), resulting in a propeller-type polarization profile [frame (viii)]. Rosette-shaped CCTs as shown in frames (vi) and (x) arise due to unequal amplitudes of the two colors in the corresponding sub-pulses.

equal amplitude, the CCT describes a Lissajous-curve with characteristic ($3\omega : 4\omega$) symmetry. For the first pre- and post-pulse [of the overall pulse sequence; frames (ii) and (iv)] the CCTs capture only the *s*-polarized red component (ω_1). The second pre- and post-pulse again describe ($3\omega : 4\omega$) Lissajous-curves [frames (i) and (v)], now compressed in *x*-direction by a factor of $J_2(1.43)/J_1(1.43) \approx 0.4$ corresponding to the amplitude ratio of the contributing sub-pulses. While the second post-pulse oscillates in-phase with the main pulse, the second pre-pulse is mirrored in *y*-direction due to the above mentioned π phase shift in the *p*-component resulting from the symmetry relation of the Bessel functions.

By use of a QWP behind the shaper setup, the O-LP field is converted into a phase-modulated CNR-CP bichromatic field. Since the QWP mixes both colors, their contributions to the temporal field are no longer disentangled. Figure 3(d) shows the measured second order CC for the p -component of the modulated CNR-CP field. The CC trace displays a multi-pulse sequence with a sub-pulse separation of 90 fs. The interferometric CC of the main pulse exhibits a beating pattern best seen in the enhancement in Fig. 3(e) where the measured beating envelopes are shown in addition. The corresponding CCT in frame (viii) describes a propeller with c_7 symmetry similar to the one in Fig. 2(c). For the first pre- and post-pulse, the interferometric CC oscillates with the carrier frequency ω_1 since there is no interference with the blue component. In accordance with the circular polarization of the red component, the CCTs in frames (vii) and (ix) describe circles. For the second pre- and post-pulse the interferometric CC also exhibits a beating. In this case, however, the beating contrast is reduced due to the unequal amplitudes of red and blue component. This leads to the rosette-shaped CCTs shown in frames (vi) and (x). Generally, the propeller shapes in frames (vi)-(x) derive from the corresponding Lissajous-curves in frames (i)-(v) by application of the QWP, mathematically described by the matrix in Eq. (10).

2.3.3. CEP stability and control

The CEP of few-cycle laser pulses is a central control parameter in attosecond (as) science [44–47]. It is used e.g. to steer the motion of free electrons in as-pulse generation via high harmonic generation (HHG) [48–51] or to manipulate the dynamics of bound electrons in atoms and molecules [52–54]. The physical mechanism behind these processes often relies on a Brumer-Shapiro-type control scheme based on the interference of M - vs. N -photon excitations [13]. When frequency-multiplied light from the same fundamental pulse is used, the CEP dependence of the excitation cancels [47], leaving the relative phase between the two driving fields as the basic control parameter. This is the case in many ($\omega : 2\omega$) applications where the fundamental and second harmonic of a CEP-unstable laser is used. In shaper-generated bichromatic fields, both the M - and the N -photon transition are driven by the same fundamental pulse. As discussed below [cf. Eq. (13)], this intra-pulse quantum interference is sensitive not only to the relative phase between the two colors but also to the CEP of the driving pulse. Thus, stabilization of the CEP is crucial in order to establish efficient bichromatic control schemes. In our experiments, the input WLS is actively CEP stabilized with short-term RMS fluctuations of about 260 mrad over 1 s and only marginally larger long-term fluctuations of about 270 mrad measured over 1 h [see Sec. 2.1]. To preserve the CEP stability, our shaper setup is built in a robust and compact design [15, 28] minimizing optomechanical vibrations and reducing the optical path length. The CEP stability of the bichromatic output fields is investigated using a home-built f - $2f$ -interferometer capable of single-shot measurements. By feeding the active stabilization loop of the laser system with data from the interferometer, we obtained short-term CEP fluctuations of about 270 mrad RMS over a period of 1 s, which converge to long-term fluctuations in the order of 280 mrad RMS, measured over a period of 1 h, behind the shaper. Thus, the setup increases the short-term fluctuations marginally and leaves the long-term CEP stability unaltered. Figure 4(a) displays the results of a measurement performed over 30 s. The discrete steps were introduced by the pulse shaper to demonstrate shaper-based CEP control. For this purpose, we applied constant phase functions of the form $\varphi_n(\omega) \equiv \phi_{CE}$ (for $n = 1, 2$) to the LC-SLM. Switching the CEP between $\phi_{CE} = 0$ and π during the first 20 s, or $\phi_{CE} = 0$ and $\pi/2$ in the last 10 s, is clearly visible in the data. CEP-overshoots following every switching event are due to the re-alignment of the liquid crystals.

In addition, the shaper-based CEP control was verified by temporal characterization of the output fields via second order CC including the measurement of carrier and envelope. The results are shown in Figs. 4(b)-(d). The left column displays CC traces of the linearly (p) polarized compressed few-cycle pulse, obtained when no amplitude modulation is applied to the WLS.

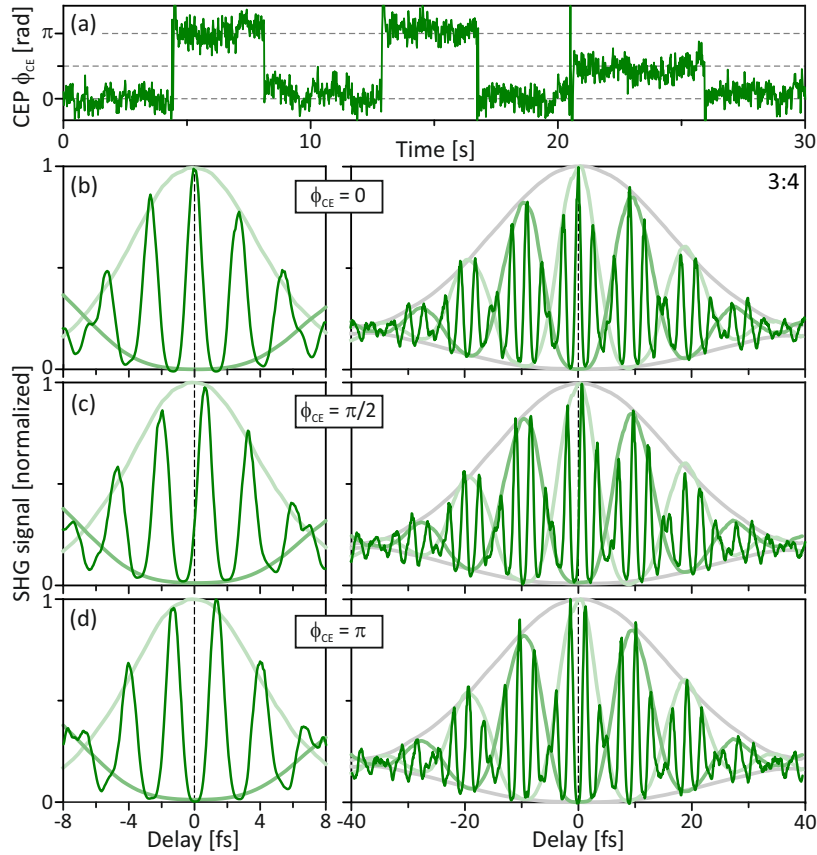


Fig. 4. Pulse shaper control of the CEP. (a) CEP fluctuations measured behind the shaper using an f - $2f$ -interferometer. The discrete steps indicate active switching of the CEP via the LC-SLM. (b)-(d) Temporal characterization of the output fields for different values of the CEP ϕ_{CE} . Left: Few-cycle pulses obtained from the compressed WLS with no amplitude modulation applied. Right: Results for a bandwidth-limited ($3\omega : 4\omega$) CNR-CP bichromatic pulse.

For $\phi_{CE} = 0$ the interferometric CC (darkgreen line) in Fig. 4(b) displays a $\Delta t = 5.3$ fs pulse with a cosine carrier oscillation. Varying the CEP to $\phi_{CE} = \pi/2$ and π results in sine and negative cosine carrier oscillations as shown in Figs. 4(c) and (d), respectively. The right column shows the results obtained for the bandwidth-limited ($3\omega : 4\omega$) CNR-CP bichromatic field already discussed in Sec. 2.3.1 [cf. Figs. 2(c) and (e)]. Also, in this case, the carrier oscillation is accurately controlled by choice of ϕ_{CE} . For ($M\omega : N\omega$) CNR-CP fields, shifting the CEP corresponds to a rotation of the resulting propeller pulse about the propagation axis by the angle

$$\alpha_{M,N}(\phi_{CE}, \phi_1, \phi_2) = \frac{N \cdot (\phi_{CE} + \phi_1) - M \cdot (\phi_{CE} + \phi_2)}{M + N}. \quad (13)$$

The rotation direction, i.e. the sign of $\alpha_{M,N}$, depends on the helicity of the two colors. According to Eq. (13), the relative phases of red ($\omega_1 = M\delta\omega$) and blue ($\omega_2 = N\delta\omega$) spectral bands, ϕ_1 and ϕ_2 , respectively, rotate the propeller in opposite directions. For $N > M$, rotation by the phase ϕ_1 is more effective compared to ϕ_2 . In addition, Eq. (13) reveals that the CEP rotates the propeller in the ϕ_1 -direction, however at a lower rate of $(N - M)/(M + N) \cdot \phi_{CE}$. Since the angle is affected by CEP fluctuations, coherent control experiments based on the interference of

N vs. M -photon excitation using shaper-generated bichromatic fields require a stable CEP.

Overall, the results presented in Secs. 2.3.1-2.3.3 highlight the capability of the shaper-based approach to generate high-fidelity polarization-shaped bichromatic fields with low-order (commensurable) frequency ratio from a CEP-stable WLS. The CEP is maintained and accurately controlled by the setup. Combined spectral phase and amplitude modulation of the WLS enables both the generation of waveform-controlled few-cycle pulses and the design of tailored bichromatic fields.

3. Summary and conclusion

In this paper, we demonstrated an optical scheme for amplitude and phase modulation of octave-spanning CEP-stable WL supercontinua to generate ultrashort polarization-tailored bichromatic fields. By adapting a $4f$ polarization pulse shaper to the ultrabroadband WLS, and making use of a composite polarizer in the Fourier plane for independent modulation of two orthogonally polarized spectral bands, we were able to generate bichromatic fields with low-order commensurable center frequencies. Shaper-based CC measurements revealed the temporal structure and the Lissajous-/propeller-type polarization profiles of the generated O-LP and CNR-CP bichromatic fields. Unlike interferometric setups, the shaper-based scheme provides inherent phase stability of the two colors due to the common-path geometry. The CEP stability behind the shaper is preserved owing to the robust and compact design of the setup. The presented scheme offers full control over all bichromatic parameters such as the frequency ratio, the amplitude ratio, the bandwidth and the polarization state of both colors. Moreover, the additional phase modulation modality provides us with the complete toolbox of femtosecond pulse shaping [35, 55, 56] individually applicable to each color. The output waveform can be controlled by tuning the CEP or by adjusting the relative phase and time delay between the two colors with zeptosecond precision [15]. More generally, the freedom to shape the spectral phase and amplitude of both bands individually allows to design tailor-made bichromatic fields of unprecedented versatility, making our approach especially attractive for observation and coherent control of ultrafast dynamics. Generally, high-fidelity spectral amplitude and phase-modulation of CEP-stable ultrabroadband WL supercontinua opens up a new class of polarization-tailored ultrashort laser pulses and provides new perspectives for the generation of accurately controlled few-cycle waveforms. Due to the enormous bandwidth of the WL of about 1.6 eV at the central photon energy of 2 eV, bichromatic polarization shaping enables high precision polarization-sensitive two-color pump-probe experiments with phase-locked CEP-stable laser pulses at a broad range of excitation wavelengths. Currently, we employ polarization-shaped bichromatic fields in studies on bichromatic control of ultrafast electron dynamics via M - vs. N -photon interference of states with different parity. Further applications of polarization-shaped bichromatic laser fields include coherent control of HHG as theoretically suggested by [1] along with refined studies of the multiphoton photoelectron circular dichroism of chiral molecules [57] in order to clarify the underlying physical mechanism.

Funding

Deutsche Forschungsgemeinschaft (DFG) (501100001659) via the priority programme SPP1840-QUTIF.